MICHIGAN STATE
UNIVERSITY

National Superconducting Cyclotron Laboratory

ANGULAR DISTRIBUTIONS OF γ-RAYS WITH INTERMEDIATE-ENERGY BEAMS

HEATHER OLLIVER, THOMAS GLASMACHER, and ANDREW STUCHBERY

MSUCL-1271 AUGUST 2003

Accepted for publication in Physical Review C

Angular Distributions of γ-rays with Intermediate-Energy Beams

Heather Olliver,[1,2,*] Thomas Glasmacher,[1,2] and Andrew E. Stuchbery[1,3]

[1]*National Superconducting Cyclotron Laboratory, Michigan State University, East Lansing, Michigan 48824*

[2]*Department of Physics and Astronomy, Michigan State University, East Lansing, Michigan 48824*

[3]*Department of Nuclear Physics, Research School of Physical Sciences and Engineering, The Australian National University, Canberra, ACT 0200, Australia.*

(Dated: August 26, 2003)

Abstract

The feasibility of measuring angular distributions of γ-rays emitted from intermediate-energy exotic nuclei to determine multipolarities of γ-ray transitions is shown. Plots of γ-ray angular distributions for various excitation mechanisms are presented. The influences of the percentage of alignment in an excited state, the beam velocity, the spins of the initial and final states, the minimum impact parameter, the atomic number and mass of the projectile and target and the excitation energy are discussed. The aim is to illustrate that γ-ray angular distribution experiments can be succesfully performed with intermediate-energy beams.

PACS numbers: 23.20.En; 25.70.Mn; 25.70.De; 25.60.-t

Keywords: γ-ray angular distributions; exotic nuclei; intermediate-energy exotic beams; fragmentation, nucleon-knockout and Coulomb excitation reactions; alignment; spin assignments

*olliver@nscl.msu.edu

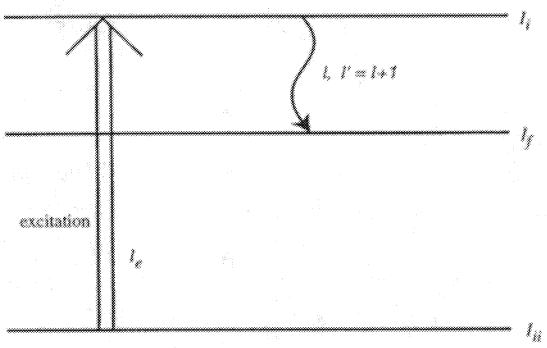

FIG. 1: Notation used in this article. I_i and I_f are the initial (excited) and final spins of the γ-ray transition, respectively. The lowest possible multipolarities of the γ-ray transition are l and $l' = l+1$. I_{ii} is the spin of the initial state before the nucleus is excited and l_e is the orbital angular momentum of the excitation.

I. INTRODUCTION

Measuring angular distributions of γ-rays emitted from excited nuclei is an important tool in nuclear structure studies because of the ability to unambiguously assign multipolarities of γ-ray transitions. In-beam techniques are well established for beams with energies near the Coulomb barrier (see for example [1]), but have not been thoroughly investigated for intermediate-energy ($v/c \approx 0.3 - 0.8$) exotic beams. This paper illustrates the effect of various quantities on the anisotropy of γ-ray angular distributions and indicates the feasibility of distinguishing different multipolarity γ-ray transitions using intermediate-energy exotic beams and various excitation methods.

II. NOTATION

Angular distribution function

The γ-ray angular distribution function $w_{cm}(\theta_{cm})$ specifies the relative probability to observe, in the center of mass, a γ-ray transition from spin I_i to I_f at an angle θ_{cm} with respect to the beam axis and has the form

$$w_{cm}(\theta_{cm}) = \sum_{\substack{\lambda=0 \\ \lambda \text{ even}}}^{2l'} A_\lambda B_\lambda P_\lambda(\cos(\theta_{cm})). \tag{1}$$

In this article, the notation of Krane [2] is used. Figure 1 shows the initial, I_i, and final, I_f, spins of a γ-ray transition and the lowest possible multipolarities of the γ-ray, l and $l' = l+1$. I_{ii} is the spin of the initial state before the nucleus is excited and l_e is the orbital angular momentum of the excitation. The A_λ coefficients (defined in equation 6) depend on l, l', I_i and I_f. The B_λ coefficients (defined in equation 9) depend on I_{ii}, I_i and l_e. The $P_\lambda(\cos(\theta_{cm}))$ terms in equation 1 are Legendre polynomials. Only the even ordered Legendre polynomials contribute to $w_{cm}(\theta_{cm})$ because γ-ray decay is an electromagnetic process in which parity is conserved. To Lorentz boost $w_{cm}(\theta_{cm})$ into the laboratory frame, a solid angle correction

is applied and the Legendre polynomials are written as a function of the laboratory frame angle θ with respect to the beam axis. Thus,

$$w(\theta) = \sum_{\substack{\lambda=0 \\ \lambda \text{ even}}}^{2l'} A_\lambda B_\lambda P_\lambda(\cos(\theta_{cm})) \frac{1-\beta^2}{(\beta\cos(\theta)-1)^2}, \tag{2}$$

where $\cos(\theta_{cm})$ can be transformed to $\cos(\theta)$ in the laboratory frame using the relation

$$\cos(\theta_{cm}) = \frac{\cos(\theta)-\beta}{1-\beta\cos(\theta)}. \tag{3}$$

β is the velocity of the center-of-mass frame with respect to the laboratory frame relative to the speed of light. For $\beta = 0$, $w(\theta)$ is equal to $w_{cm}(\theta_{cm})$. The angular distribution functions in equations 1 and 2 are not necessarily normalized. Dividing by $4\pi A_0 B_0$ normalizes $w(\theta)$ and $w_{cm}(\theta_{cm})$ to unity, with respect to integrating over all space, because the even Legendre polynomials of order two and greater integrate to zero over the interval $0 \leq \theta \leq \pi$. If equations 6 through 9 are used and $P(m)$ is normalized, A_0 and B_0 are unity. If $P(m)$ is not normalized, as in equation 12 for intermediate-energy Coulomb excitation because $P(m)$ is dependent on λ, then dividing by B_0 is necessary to normalize the angular distribution function. The normalized angular distribution function $W(\theta)$ has the form

$$W(\theta) = \frac{w(\theta)}{4\pi A_0 B_0} = \frac{1}{4\pi}\left[1 + \sum_{\substack{\lambda=2 \\ \lambda \text{ even}}}^{2l'} \frac{A_\lambda B_\lambda P_\lambda(\cos(\theta_{cm}))}{A_0 B_0}\right] \times \frac{1-\beta^2}{(\beta\cos(\theta)-1)^2}, \tag{4}$$

and is normalized to

$$\int_\Omega W(\theta)\, d\Omega = 1. \tag{5}$$

Normalizing $w_{cm}(\theta_{cm})$ is similarly performed. The sums in equations 1, 2 and 4 extend to twice the multipolarity of the γ-ray transition, $l' = l+1$, with the odd λ terms equal to zero. In equations 1, 2 and 4, A_λ are angular distribution coefficients with the form

$$A_\lambda = \frac{1}{1+\delta^2}\left(F_\lambda(l,l,I_f,I_i) + 2\delta F_\lambda(l,l',I_f,I_i) + \delta^2 F_\lambda(l',l',I_f,I_i)\right). \tag{6}$$

These angular distribution coefficients consider only two multipolarities, l and $l' = l+1$, contributing to the γ-ray transition. In this article those multipolarities correspond to the lowest two multipolarities that are allowed by angular momentum coupling. The mixing ratio, δ is defined as

$$\delta = \frac{< I_f||\pi(l+1)||I_i >}{< I_f||\pi'(l)||I_i >}, \tag{7}$$

where π and π' specify the type of radiation, electric or magnetic. The ordinary F-coefficients are defined as

$$F_\lambda(l,l',I_f,I_i) = (-1)^{I_f+I_i+1}(2\lambda+1)^{1/2}(2l+1)^{1/2} \times (2l'+1)^{1/2}(2I_i+1)^{1/2}\begin{pmatrix} l & l' & \lambda \\ 1 & -1 & 0 \end{pmatrix}\begin{Bmatrix} l & l' & \lambda \\ I_i & I_i & I_f \end{Bmatrix}. \tag{8}$$

This is the limiting case of the generalized F-coefficients [3] when only one γ-ray is observed with respect to a fixed direction. For the illustrative purposes of this article, only pure transitions of multipolarity l are considered. For pure transitions where l is the only multipolarity that contributes to the γ-ray transition $A_\lambda = F_\lambda(l, l, I_f, I_i)$. The B_λ coefficients in equations 1, 2 and 4, are orientation parameters which have the form

$$B_\lambda = (2\lambda+1)^{1/2}(2I_i+1)^{1/2} \sum_{m=-I_i}^{I_i} (-1)^{I_i+m} \times \begin{pmatrix} I_i & I_i & \lambda \\ -m & m & 0 \end{pmatrix} P(m). \quad (9)$$

As can be seen in equation 9, the B_λ coefficients are directly related to the population parameters *P(m)*, which specify the initial m substate distribution of a nucleus in an excited state with spin I_i and are related to the amount of alignment in the excited state. A nucleus in an excited state with 100% alignment means that the angular momentum of the nucleus is fully oriented either perpendicular to or parallel and anti-parallel to the beam axis. As reviewed in [5], a percentage of alignment quoted as less than 100% is measured or calculated with respect to the B_2 value for the fully aligned cases. Figure 2 illustrates the effect of the Lorentz boost on $W(\theta)$ for beam velocities of $\beta = 0.4$ and $\beta = 0.6$ with complete oblate or prolate alignment, defined below. It will be seen that a Lorentz boost for $\beta = 0.4$ or 0.6 has a smaller effect on $W(\theta)$ than a reduction in the alignment of an excited state. The amount of alignment in an excited state and the Lorentz boost are independent and have different effects on $W(\theta)$. A reduction in the amount of alignment in an excited state reduces the anisotropy of $W(\theta)$ and a Lorentz boost forward focuses $W(\theta)$. A related paper [5] discusses the general formalism of γ-ray angular correlation and angular distribution measurements.

Alignment

The alignment produced in a nucleus in an excited state can be one of two types. If the angular momentum of the nucleus is aligned perpendicular to the beam axis, then the $m = 0$ substates are preferentially populated. This oblate alignment is observed in fusion-evaporation (heavy-ion, xn) reactions. If the angular momentum of the nucleus is aligned parallel and anti-parallel to the beam axis, then the $m = \pm I_i$ substates are preferentially populated. This is referred to as prolate alignment. A prolate-aligned nucleus produces a different γ-ray angular distribution for a given γ-ray transition than an oblate-aligned nucleus. Three-dimensional plots of W(θ) are shown in Figure 3. The first row shows a pure quadrupole transition, the second row a pure dipole transition and the third row a pure octupole transition. The first column shows the transitions at rest with 100% oblate alignment. The second column shows the transitions at $\beta = 0.4$ with 100% oblate alignment. The third column shows the transitions at $\beta = 0.4$ with 20% oblate alignment. As can be seen in the last column of Figure 3, a reduction in the percentage of alignment combined with a Lorentz boost for $\beta = 0.4$ washes out much of the anisotropy in the γ-ray angular distribution. A similar reduction in anisotropy occurs in the γ-ray angular distribution for a prolate aligned nucleus. However, distinguishing quadrupole, dipole and octupole transitions is still experimentally possible and will be discussed quantitatively in section IV.

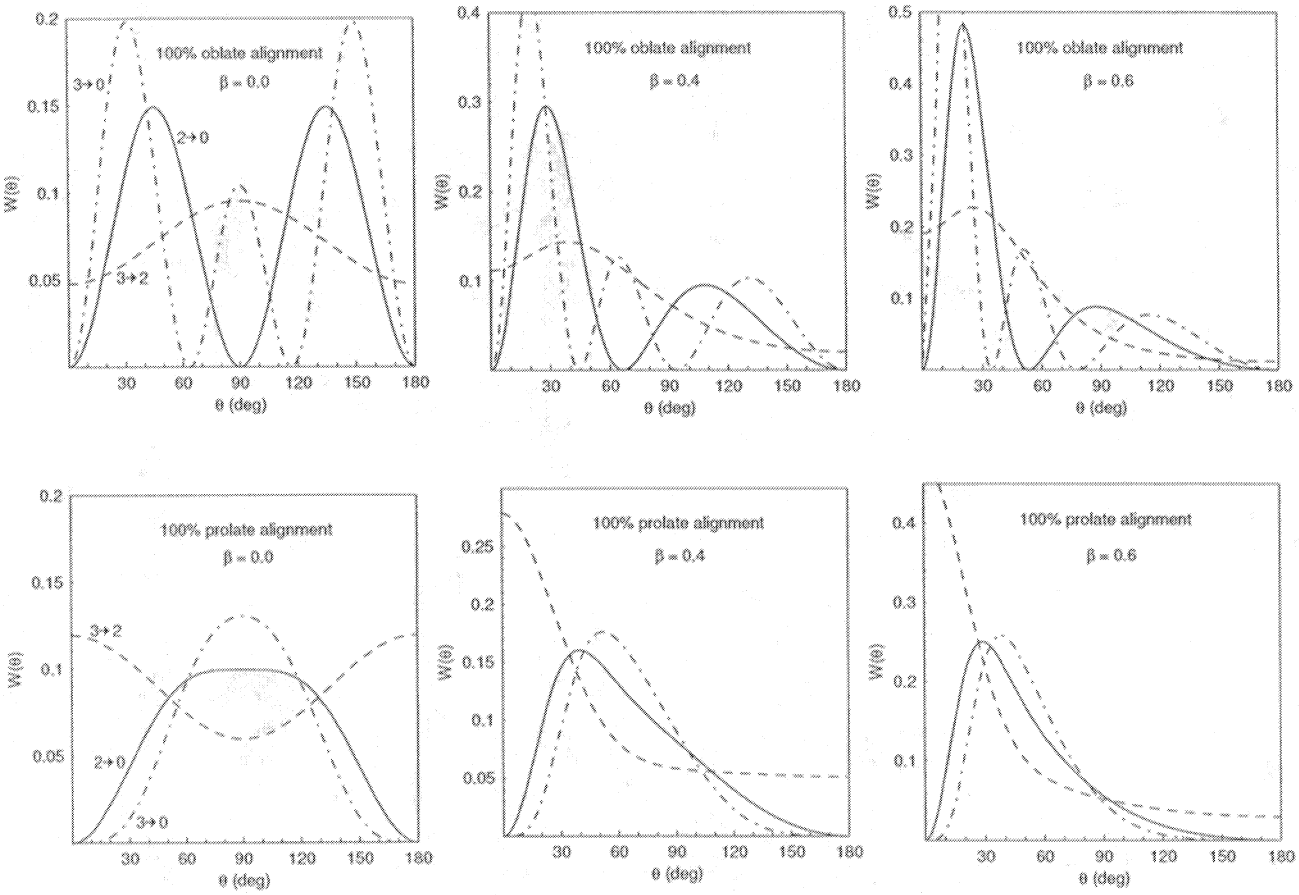

FIG. 2: Plots of $W(\theta)$ at $\beta = 0.0$, 0.4 and 0.6 for quadrupole (solid curves), dipole (dashed curves) and octupole (dash-dotted curves) transitions with 100% oblate or prolate alignment.

III. TRANSITIONS OF IDENTICAL MULTIPOLARITY

Examples of 4→2 and 2→0 quadrupole transitions at 100% and 50% oblate or prolate alignment are shown in Figure 4. For 100% prolate alignment different spin $I_i \to I_f$ transitions with the same multipolarity are nearly identical at $\beta = 0.4$. Angular distributions for quadrupole 2→0 and 4→2 transitions are equivalent, for dipole 3→2 and 1→0 are equivalent and for octupole 6→3 and 3→0 are equivalent. However, for 100% oblate alignment those same three pairs of transitions are significantly different. The 1→0, 2→0 and 3→0 transitions vanish at the origin and have more features than the 3→2, 4→2 and 6→3 transitions, respectively. As the amount of oblate alignment decreases, the same-multipolarity different-spin $I_i \to I_f$ transitions become more alike. As the amount of prolate alignment decreases, same-multipolarity different-spin $I_i \to I_f$ transitions do not all approach an isotropic Lorentz-boosted distribution the same way, but the differences between those same multipolarity transitions are small enough not to impede distinguishing quadrupole, dipole and octupole transitions.

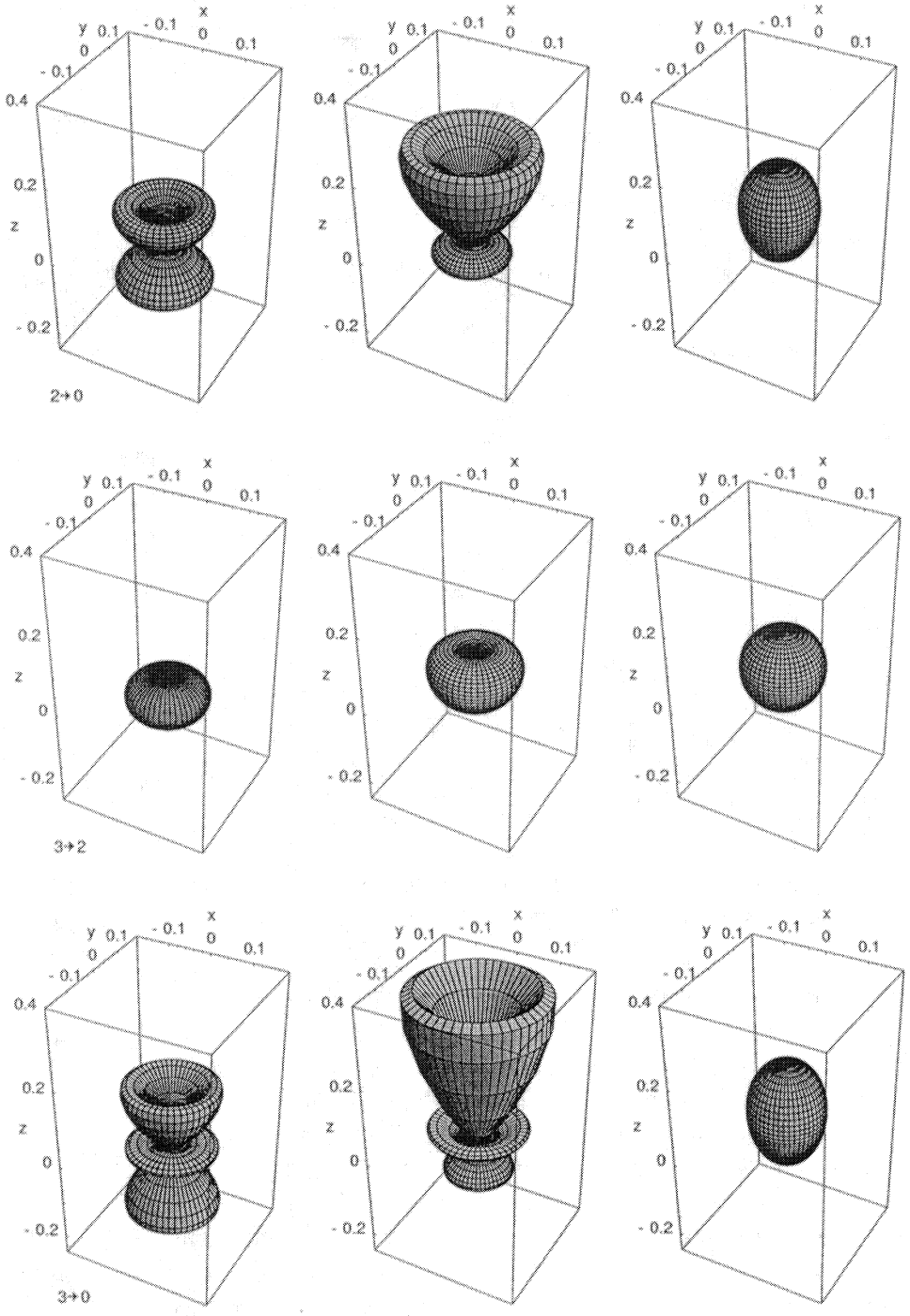

FIG. 3: Three-dimensional γ-ray angular distributions for three γ-ray transitions from an initial state with oblate alignment. The top row of figures shows pure quadrupole transitions (2→0), the second row shows pure dipole transitions (3→2) and the third row shows pure octupole transitions (3→0). The first column shows all three transitions, quadrupole, dipole and octupole, at $\beta = 0.0$ with 100% oblate alignment. The second column shows the same transitions Lorentz boosted for $\beta = 0.4$. The last column shows the same transitions Lorentz boosted for $\beta = 0.4$ and with the alignment reduced to 20% oblate alignment. In all the plots, the beam axis is the z-axis with the beam direction towards positive z.

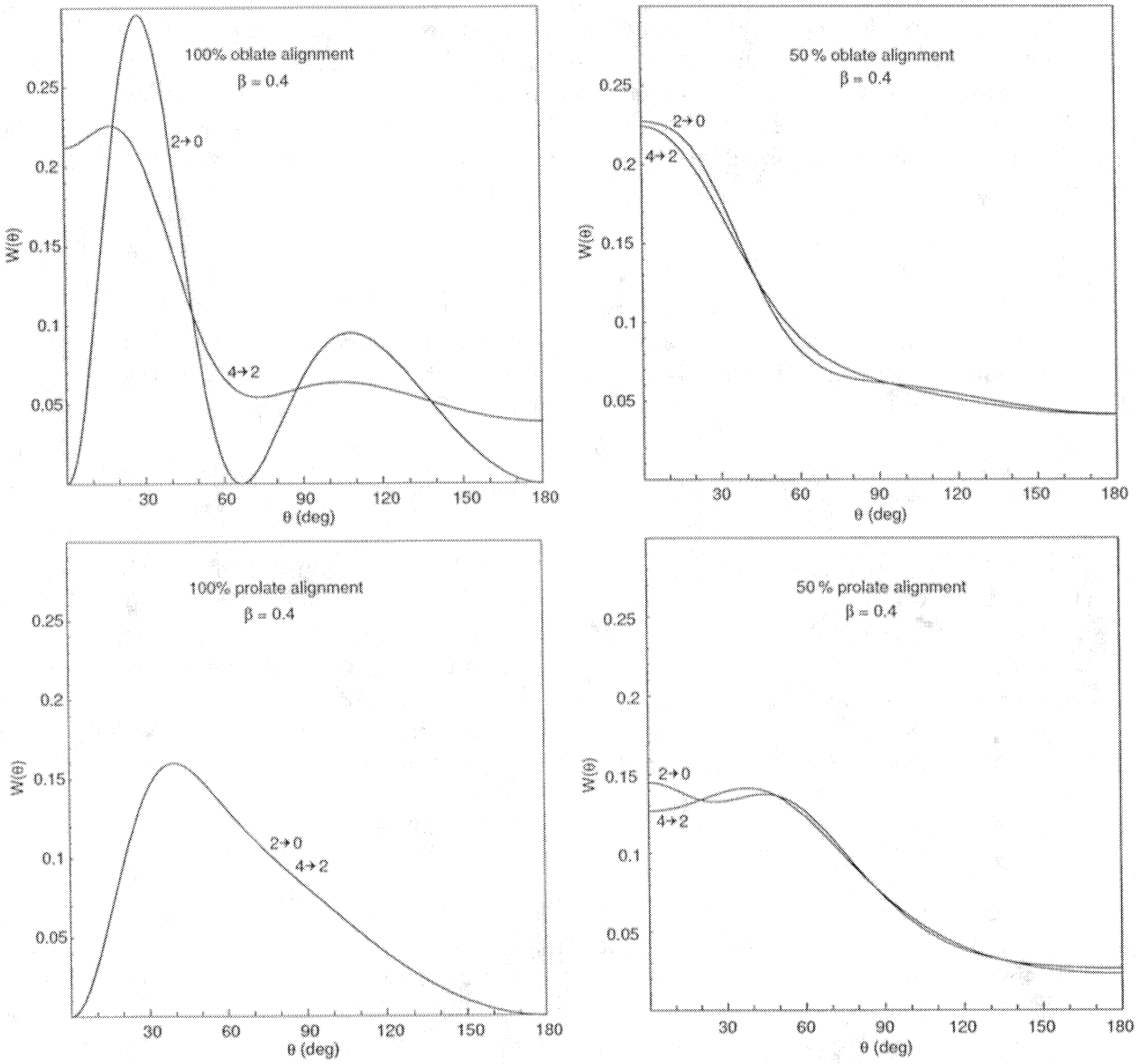

FIG. 4: Plots of $W(\theta)$ for 100% and 50% oblate or prolate alignment for two different quadrupole transitions at $\beta = 0.4$. The top row shows that 4→2 and 2→0 transitions are significantly different at 100% oblate alignment. However, at 50% alignment they are similar. The bottom row shows that 4→2 and 2→0 transitions are identical with 100% prolate alignment and at 50% alignment they are similar. The dipole transitions, 3→2 and 1→0, and the octupole transitions, 6→3 and 3→0, behave similarly to the two quadrupole transitions shown.

IV. DIFFERENT REACTION MECHANISMS

In an in-beam experiment, partial alignments will be observed. Four reaction mechanisms, namely fusion evaporation, fragmentation, knockout and intermediate-energy Coulomb excitation, will be discussed here. The latter three have become standard in-beam spectroscopy tools with γ-ray detection, using intermediate-energy ($\beta = 0.3$–0.8) exotic beams, but have

not been thoroughly explored. Fragmentation reactions were pioneered in 1979 [6], but did not utilize γ-ray detection in the early implementations. Nuclear break-up reactions (including fragmentation and nucleon-knockout reactions) were first used in conjunction with the detection of γ-rays as a spectroscopic tool in three pioneering experiments [7–9]. The first intermediate-energy Coulomb excitation experiments were performed in 1995 [7, 10].

Fusion evaporation

Non-relativistic fusion evaporation reactions will first be discussed. Yamazaki [11] approximated the population parameter *P(m)*, in equation 9, for non-relativistic (heavy-ion, xn) reactions using a Gaussian distribution centered at $m = 0$, based upon work done by Diamond *et al.* [12]. Normalized, *P(m)* then has the form

$$P(m) = \frac{e^{-m^2/2\sigma^2}}{\sum_{n=-I_i}^{I_i} e^{-n^2/2\sigma^2}}. \tag{10}$$

The width of the Gaussian distribution, σ, is related to the amount of oblate alignment in the excited state. For an excited state with less than 100% alignment, $\sigma > 0$ such that $B_2/B_2^{max} \times 100$ is equal to the percentage of alignment, where B_2^{max} is the B_2 coefficient corresponding to the fully aligned case. We have reproduced the tabulated angular distribution coefficients of Yamazaki [11] and der Mateosian and Sunyar [13]. A reduction in the amount of alignment produced in a nucleus in an excited state significantly decreases the anisotropy of the γ-ray angular distribution as seen previously for oblate alignment in Figure 3.

Fragmentation reactions

With the intermediate-energy beams available today, fragmentation reactions have become a spectroscopic tool for creating and studying exotic nuclei. In fragmentation reactions the amount and type of alignment produced is not well studied. Investigations of alignment and polarization produced in intermediate-energy fragmentation reactions [14–17] are not consistent. The alignment produced in [15–17] ranges from less than 1% to 35%. In the experiment where less than 1% alignment was produced [15], the fragment was five protons and ten neutrons removed from the incoming projectile so little alignment was expected. This is because each of the 15 nucleons carried off some amount of linear and angular momentum in a random direction, thus leaving the fragment with a significantly lower angular momentum and destroying the alignment. Reactions using intermediate-energy beams were ^{9}Be(^{22}Ne,^{18}N)X [15], ^{9}Be(^{18}O,^{14}Bγ)X [17], ^{12}C(^{13}C,^{12}B)X [15] and ^{9}Be(^{46}Ti,^{43m}Scγ)X [16]. The first two reactions were performed at 60 MeV/nucleon and were $3p1n$ removal reactions. In those two reactions, 14.4% prolate alignment and less than 5% prolate or oblate alignment, respectively, were observed in the center of the longitudinal momentum distribution. In the wings of the momentum distributions, oblate alignment was observed in both experiments. In ^{12}C(^{13}C,^{12}B)X [15], 4.7% prolate alignment was observed in the center of the momentum distribution. In ^{9}Be(^{46}Ti,^{43m}Scγ)X [16], performed at 500 MeV/nucleon, 35% prolate alignment was observed in the center of the momentum distribution and 15% oblate alignment was observed in the wing of the momentum distribution. Though the magnitudes of the alignment observed differ significantly, the type of alignment produced as a function of

the longitudinal momentum distribution is consistent. In [15–17] the alignments produced from the reactions were prolate in the center of the momentum distributions and oblate in the wings (or tail) of the momentum distributions. This can be understood in terms of a simple kinematical model [16, 17] where the projectile fragment acts as a spectator while the nucleons in the overlapping volume with the target are removed. The outgoing momentum of the fragment is then directly related to the angular momentum of the fragment, thus giving prolate or oblate alignment values. Reactions where more nucleons are removed have broader momentum distributions [18]. Thus the m substate distributions are flatter, resulting in less alignment. This supports the result in [15] where 15 nucleons were removed and less than 1% alignment was observed. In contrast to the above experiments, in [14] an alignment of 30%–70% was observed, though the type of alignment was not reported. The reaction was ^{9}Be(^{48}Ca,^{46}Arγ)X at 60.3 MeV/nucleon. In addition to ^{46}Ar, many of the fragments from the reaction were analyzed. In order to reproduce the approximate ratios of the γ-ray intensities of the quadrupole and dipole transitions in Figure 2 of [14], we had to assume oblate alignment. The ratios observed in [14] seem to be incompatible with any percentage of prolate alignment.

Extending the formalism of Yamazaki [11] and Diamond *et al.* [12] for oblate population distributions, two Gaussian distributions centered at $m = \pm I_i$ are used for approximating prolate alignment in fragmentation reactions [5]. Normalized, *P(m)* then has the form

$$P(m) = \frac{e^{-(I_i-|m|)^2/2\sigma^2}}{\sum_{n=-I_i}^{I_i} e^{-(I_i-|n|)^2/2\sigma^2}}. \tag{11}$$

In fragmentation reactions the target is viewed as a means of removing nucleons from the projectile. Thus, we consider the center of mass frame to be the projectile frame. In order for γ-ray angular distributions to be a useful experimental tool for measuring γ-ray multiplicities and thus spins of excited states, there must be enough alignment in the excited state to distinguish between different multipolarity transitions. As the amount of alignment decreases, the difference between the angular distribution curves for different multipolarity γ-ray transitions decreases as both curves approach Lorentz-boosted, isotropic distributions. Typical intermediate-energy beam velocities (NSCL, RIKEN, GANIL) are between $0.3c$ and $0.8c$. At the proposed RIA facility [19], beams will have velocities of approximately $0.6c$. Figures 5 and 6 show plots of $W(\theta)$ calculated with 50%, 20% and 10% oblate and prolate alignment, respectively, for quadrupole, dipole and octupole transitions. The plots are shown for incoming beam velocities of $0.4c$ and $0.6c$. Table I lists the relative difference between the quadrupole and dipole transitions with 20% alignment, as seen in Figures 5 and 6, for selected angles. Table I illustrates that for a fragmentation reaction where only 20% prolate or oblate alignment is produced the difference between a quadrupole and dipole transition is large enough to distinguish between the two and to make the measurement of γ-ray angular distributions experimentally feasible. To better illustrate the large effect of the percentage of alignment on $W(\theta)$, $W(\theta)$ is shown for quadrupole, dipole and octupole transitions with 100%, 50%, 20%, 10% and 0% oblate and prolate alignment in Figures 7 and 8, respectively, at $\beta = 0.4$ and 0.6. The curves with 0% alignment are isotropic, Lorentz-boosted distributions. The curves with the most features correspond to 100% alignment. A reduction in the percentage of alignment has a much larger effect on $W(\theta)$ than a Lorentz boost for $\beta = 0.4$ or 0.6.

For $P(m)$ approximated by a gaussian distribution(s), transitions with a given multipolarity but different spins $I_i \rightarrow I_f$ are similar for approximately 50% oblate or prolate

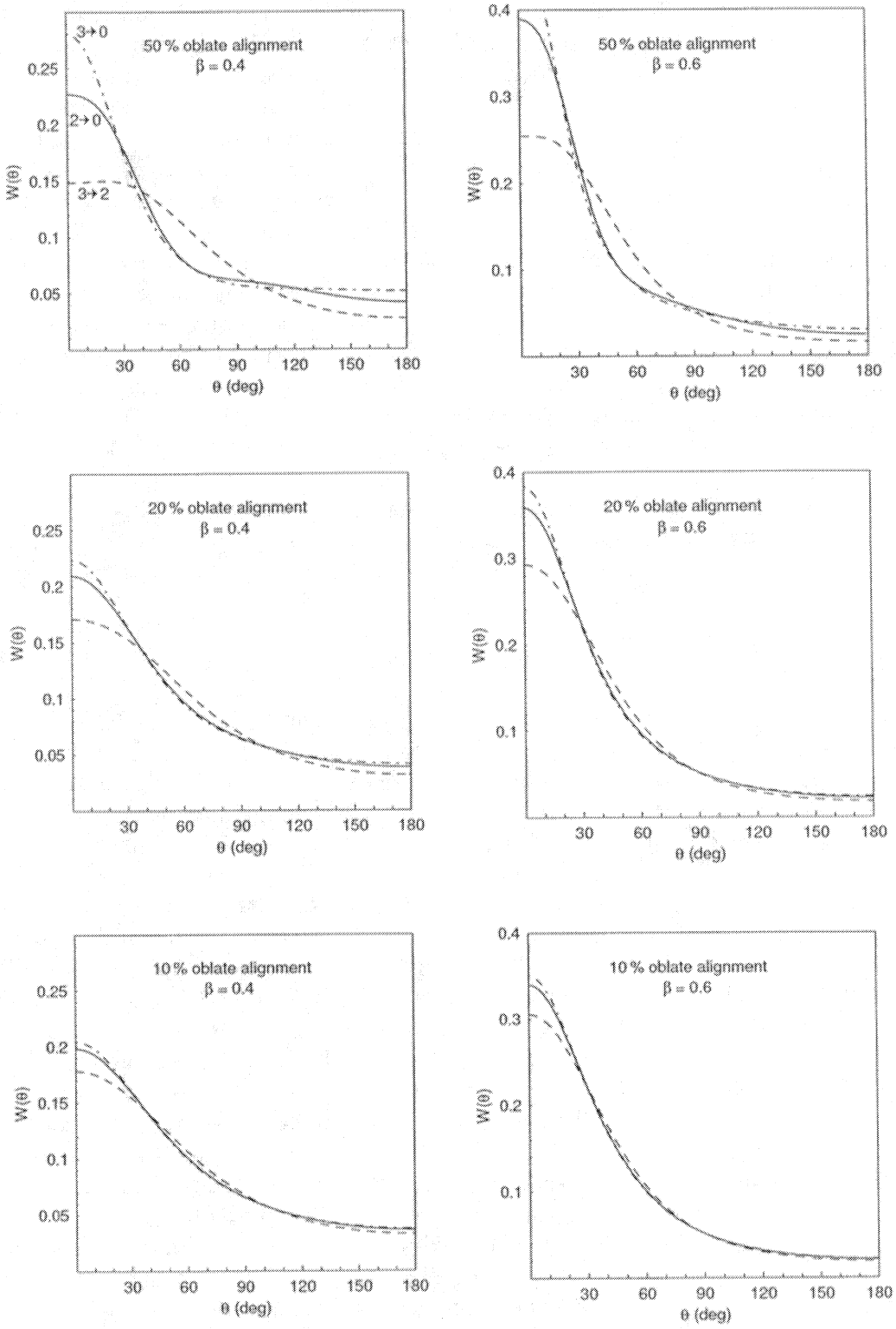

FIG. 5: Plots of $W(\theta)$ for 50%, 20% and 10% oblate alignment with an incoming beam velocity of $0.4c$ (left column) and $0.6c$ (right column). Quadrupole transitions (solid curves), dipole transitions (dashed curves) and octupole transitions (dash-dotted curves) are shown. The order of the transitions, as labeled on the upper left plot, is the same for all of the plots in the figure.

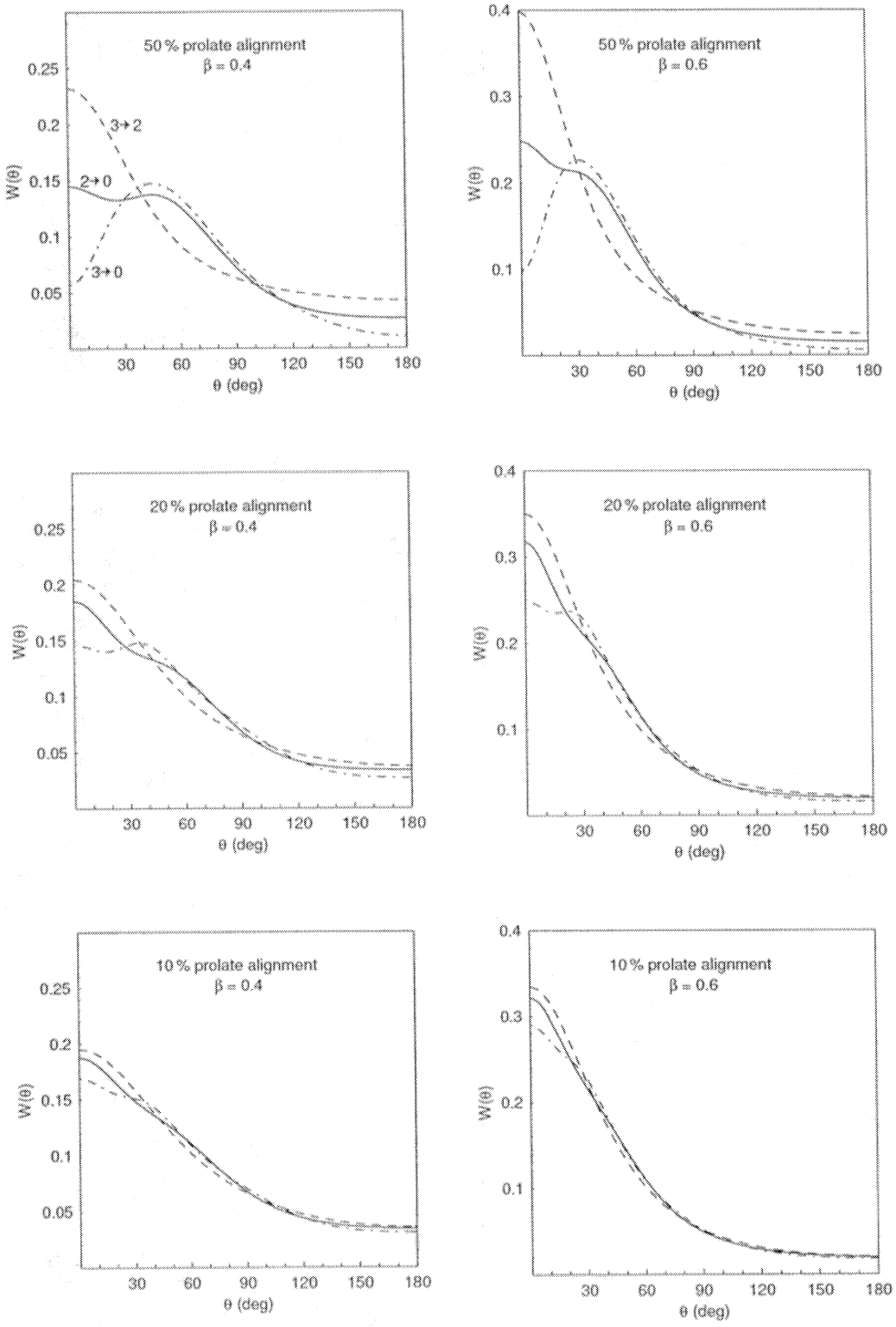

FIG. 6: Plots of $W(\theta)$ for 50%, 20% and 10% prolate alignment with an incoming beam velocity of $0.4c$ (left column) and $0.6c$ (right column). Quadrupole transitions (solid curves), dipole transitions (dashed curves) and octupole transitions (dash-dotted curves) are shown. The order of the transitions, as labeled on the upper left plot, is the same for all of the plots in the figure.

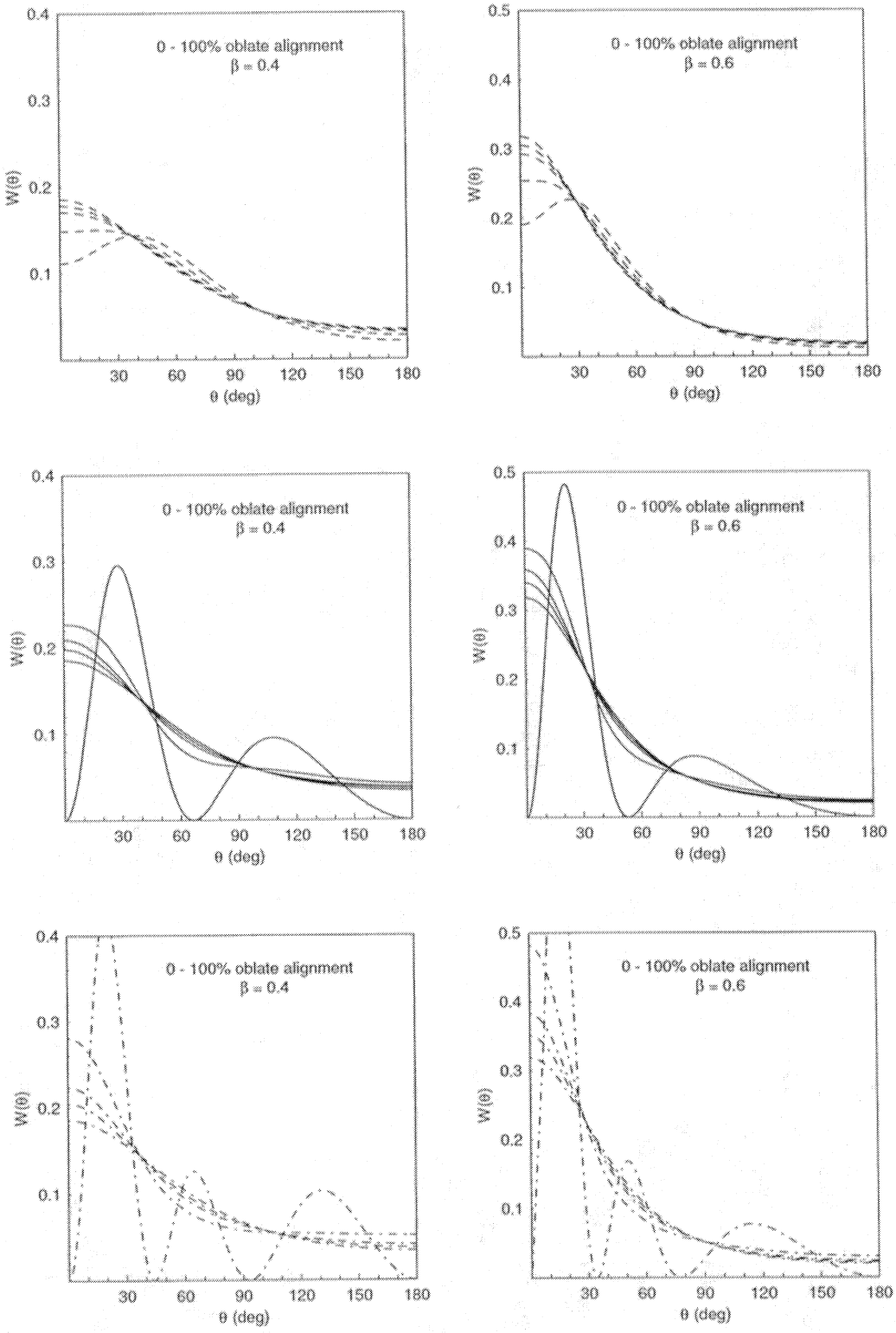

FIG. 7: Plots of $W(\theta)$ for dipole ((3→2), dashed curves, top row), quadrupole ((2→0), solid curves, middle row) and octupole ((3→0), dash-dotted curves, bottom row) transitions, each with 100%, 50%, 20%, 10% and 0% oblate alignment at $\beta = 0.4$ (left column) and 0.6 (right column). The curves with the most features are those corresponding to 100% alignment. The flatter curves are those corresponding to 0% alignment (an isotropic Lorentz-boosted distribution.)

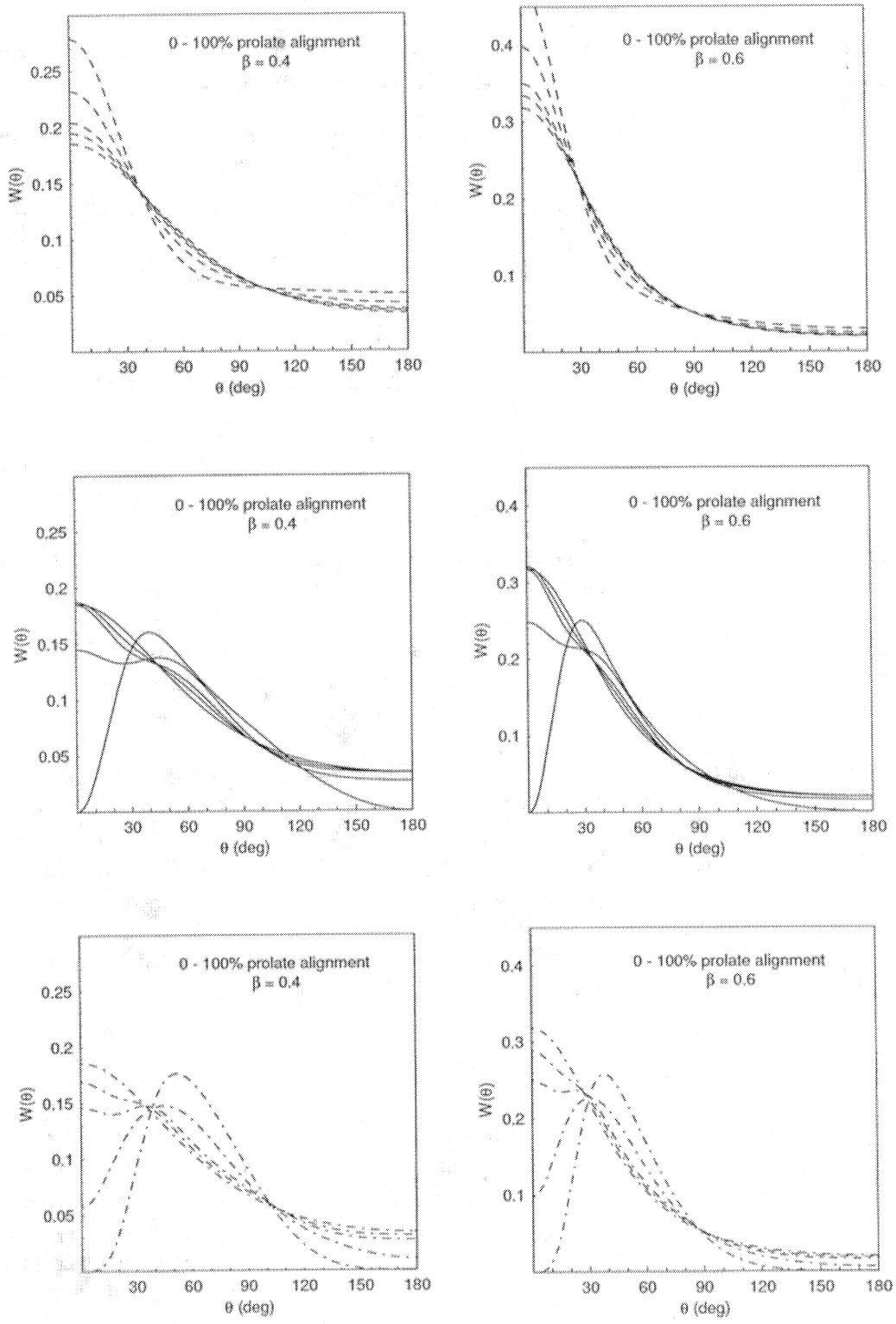

FIG. 8: Plots of $W(\theta)$ for dipole ((3→2), dashed curves, top row), quadrupole ((2→0), solid curves, middle row) and octupole ((3→0), dash-dotted curves, bottom row) transitions, each with 100%, 50%, 20%, 10% and 0% prolate alignment at $\beta = 0.4$ (left column) and 0.6 (right column). The curves with the most features are those corresponding to 100% alignment. The flatter curves are those corresponding to 0% alignment (an isotropic Lorentz-boosted distribution.)

TABLE I: Relative difference between a quadrupole, 2→0, and dipole, 3→2, transition (with respect to the dipole transition) for 20% oblate or prolate alignment at $\beta = 0.4$ and 0.6 for a few selected angles, θ, with respect to the beam axis.

		Relative difference (%)	
β	θ	Oblate	Prolate
0.4	0°	22.5	9.4
	25°	10.7	13.7
	60°	10.7	16.8
	150°	18.9	12.4
0.6	0°	22.5	9.4
	25°	4.7	10.0
	60°	10.5	16.4
	150°	20.4	11.3

alignment. Thus stretched quadrupole, dipole and octupole transitions can be distinguished from one another. In this article, the same amount of alignment in all excited states has been assumed in comparing different multipolarity transitions. Fragmentation reactions may produce different percentages of alignment for different initial spins, I_i, in the same nucleus. However, such differences are likely to be small and would only lead to ambiguities if one state was prolate-aligned and another state was oblate-aligned — a situation that is unprecedented.

To distinguish quadrupole, dipole and octupole transitions proper care must be given to detector placement. At the angles around 40° and 100°, $W(\theta)$ is the same for different multipolarity transitions at $\beta = 0.4$. Avoiding the range of angles around 40° and 100°, the relative difference between a quadrupole (2→0) and dipole (3→2) transition is on the order of 10–20% for fragmentation reactions with 20% prolate or oblate alignment at $\beta = 0.4$. A minimum of approximately 600 counts with negligible background, corresponding to an uncertainty of ±4%, in the γ-ray peak at a given angle is needed to distinguish between a quadrupole and dipole transition that are 10% different at that angle.

Nucleon-knockout reactions

The category of nucleon-knockout reactions includes the removal of one to a few nucleons. For one-nucleon knockout reactions, it is possible to calculate *P(m)*. The multipolarity, l_e, of the transition from I_{ii} to I_i is deduced from the momentum distribution of the knocked-out particle as well as knowledge of I_{ii}. (In nucleon-knockout reactions I_{ii} is usually the spin of an excited state in another nucleus, not the ground state spin of the nucleus of interest as may be implied in Figure 1.) To lowest order, *P(m)* can be calculated using an extension of the eikonal model [20] to obtain m substate dependent cross sections. The model utilizes the black-disk limit: the projectile wavefunction is unchanged throughout space except for a cylinder of a given radius where it is set to zero. This is discussed in more detail in [21]. In Figure 9, $W(\theta)$ is shown with the corresponding calculated m substate distribution [22] for the one-neutron removal reaction of ^{9}Be(^{28}Mg,^{27}Mgγ)X at $\beta = 0.4$. The anisotropy of the γ-ray angular distribution can be significantly increased by selecting momenta from

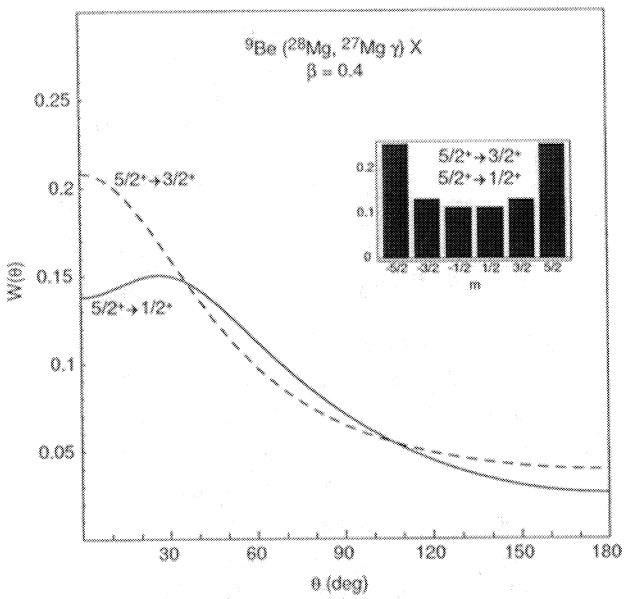

FIG. 9: $W(\theta)$ for the $1n$ knockout reaction of ^{9}Be(^{28}Mg,^{27}Mgγ)X at $\beta = 0.4$ for the $5/2^+$ to $1/2^+$ quadrupole transition and $5/2^+$ to $3/2^+$ dipole transition. The inset shows the m substate distribution for the $5/2^+$ excited state.

the center region of the momentum distribution where the greatest contribution is from the $m = \pm I_i$ substates.

The relative difference between quadrupole and dipole transitions for nucleon-knockout reactions is similar to fragmentation reactions when the entire momentum distribution is used. Thus the number of counts needed at a given angle is approximately the same as stated at the end of the previous section. If a cut is made on the center of the momentum distribution, the relative difference between quadrupole and dipole transitions can be increased significantly.

In this article, the beam axis is used as the quantization axis for calculations of γ-ray angular distributions. It has been shown [23] for nucleon-knockout reactions that if the recoil direction of the knocked-out nucleon is used as the quantization axis instead of the beam axis, a large amount of anisotropy is produced in the angular distribution. Unlike in fragmentation reactions, in nucleon-knockout reactions the excited state *P(m)* can be estimated from the momentum distribution of the knocked-out nucleon. Looking at the γ-ray angular distribution with the recoil direction as the quantization axis gives a much larger anisotropy than using the beam axis as the quantization axis and is worth pursuing further.

Intermediate-energy Coulomb excitation

In Coulomb excitation *P(m)* can be calculated from a known Hamiltonian for given electromagnetic transitions. *P(m)* can be calculated using the formalism of Alder and

Winther [24] for intermediate-energy Coulomb excitation. Its form is

$$P(m) = \sum_{\mu=-l_e}^{l_e} G_\pi(\mu,\beta,l_e)G_\pi^*(\mu,\beta,l_e)g(\mu,\xi) \times(-1)^{-m-\mu}(-1)^\lambda(2\lambda+1) \times \begin{pmatrix} I_i & I_i & \lambda \\ -m & m & 0 \end{pmatrix} \begin{pmatrix} l_e & l_e & \lambda \\ \mu & -\mu & 0 \end{pmatrix} \begin{Bmatrix} I_i & I_i & \lambda \\ l_e & l_e & I_{ii} \end{Bmatrix} \quad (12)$$

where π specifies either electric or magnetic transitions and l_e is the multipolarity of the Coulomb excitation. The $G_\pi(\mu,\beta,l_e)$ and $g(\mu,\xi)$ functions are defined in [24]. The adiabacity parameter, ξ, specifies a straight-line trajectory with a correction that takes into account that the distance of closest approach is increased due to Coulomb deflection. ξ depends on the atomic number and mass of the target and projectile, the impact parameter, the velocity of the incoming projectile, and the excitation energy of the nucleus. In the plots in figures 10 through 14 the impact parameter of the projectile is integrated from the minimum impact parameter, b_{min}, to infinity. This is experimentally realized by selecting events in which the angle of the scattered projectile is less than θ_{max}. θ_{max} is analytically related to the minimum impact parameter, b_{min}, for a specific reaction at a specific energy. In intermediate-energy Coulomb excitation reactions the target is viewed as a means of exciting the projectile. Thus, we consider the center of mass frame to be the projectile frame. With typical minimum impact parameters in Coulomb excitation (touching spheres plus a few femtometers), and excitation energies of up to a few MeV, a Coulomb-excited nucleus exhibits prolate alignment. For illustrative purposes, it is worth noting that for very large minimum impact parameters (i.e. $b_{min} \approx 100$ fm), the alignment becomes oblate. For typical impact parameters in Coulomb excitation, as the velocity of the incoming beam increases, the amount of prolate alignment increases. The angular distribution curves for ^{209}Bi(^{56}Ni,^{56}Niγ) at 85 MeV/nucleon ($\beta = 0.4$) and 233 MeV/nucleon ($\beta = 0.6$) for quadrupole, dipole and octupole transitions with their corresponding m substate distributions are shown in Figure 10.

The plots in Figures 10 through 14 are calculated with E2 and E3 excitations. A dipole transition is $I_{ii} = 0 \rightarrow I_i = 3 \rightarrow I_f = 2$ (0→3→2), quadrupole is 0→2→0 and octupole is 0→3→0. For a given multipolarity, transitions between different spins, $I_i \rightarrow I_f$, are very similar at $\beta = 0.4$ for intermediate-energy Coulomb excitation reactions.

In intermediate-energy Coulomb excitation, the effect on $W(\theta)$ of varying the minimum impact parameter, b_{min}, is negligible for typical minimum impact parameters (touching spheres plus a few femtometers). As can be seen in the top row of Figure 11 , $W(\theta)$ is shown for ^{209}Bi(^{56}Ni,^{56}Niγ) at 85 MeV/nucleon ($\beta = 0.4$) for three different minimum impact parameters: touching spheres plus 2 fm, touching spheres plus 10 fm and touching spheres plus 100 fm. The difference between $W(\theta)$ for the first two cases is minimal. In an experiment, as long as the minimum impact parameter corresponds to only Coulomb excitation reactions, the effect of the range of the minimum impact parameter used is negligible on the percentage of alignment produced. For a minimum impact parameter of touching spheres plus 100 fm, $W(\theta)$ is significantly different for each of the three transitions, however, the Coulomb excitation cross section at such a large minimum impact parameter is essentially zero. In general, as the minimum impact parameter increases, the amount of prolate alignment slowly decreases until the alignment becomes oblate. The second row of Figure 11 shows three plots of $W(\theta)$ for three different Coulomb excitation reactions. The minimum impact parameters are all touching spheres plus 2 fm. As can be seen, there is no detectable

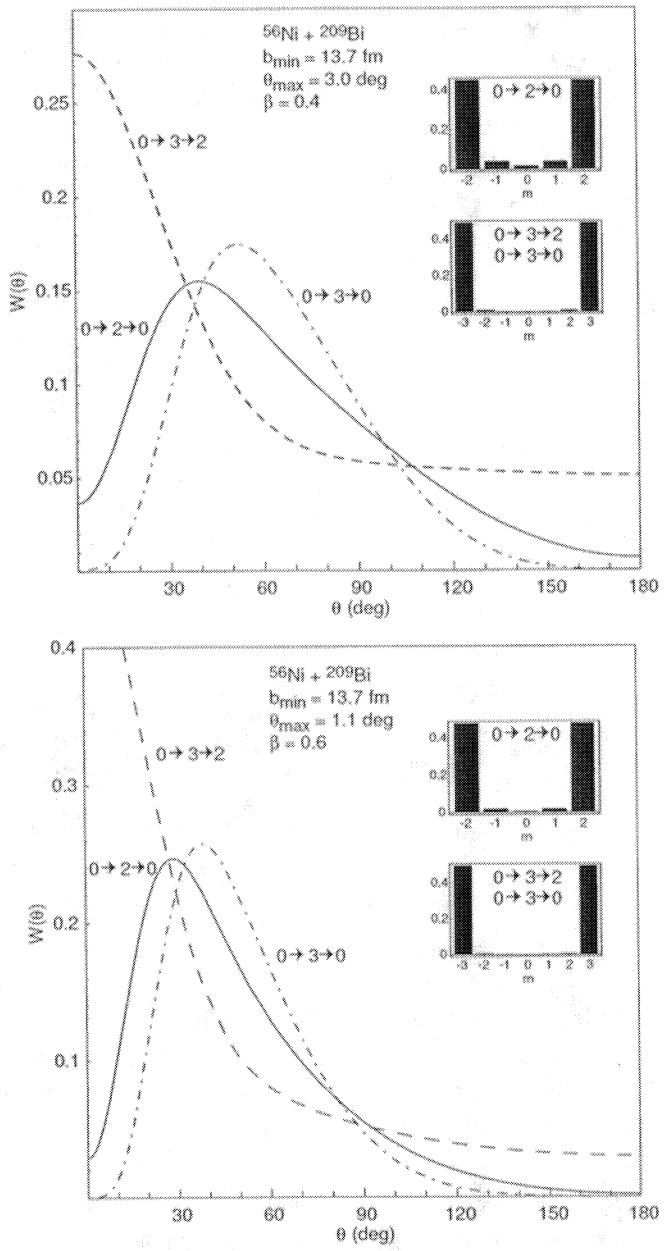

FIG. 10: $W(\theta)$ for the Coulomb excitation reaction of ^{209}Bi(^{56}Ni,^{56}Niγ) at 85 MeV/nucleon ($\beta = 0.4$) (top plot) and 233 MeV/nucleon ($\beta = 0.6$) (bottom plot) with a minimum impact parameter, b_{min}, of touching spheres plus 2 fm and an excitation energy of 1 MeV. θ_{max} is the maximum scattering angle of the projectile in the laboratory frame corresponding to b_{min}. The insets show m substate distributions for the excited states.

difference between ^{209}Bi(^{32}Mg,^{32}Mgγ), ^{209}Bi(^{44}S,^{44}Sγ) and ^{209}Bi(^{56}Ni,^{56}Niγ). For different light projectiles (from ^{14}N to ^{115}In), with a heavy (^{197}Au or ^{209}Bi) target, the effect on *P(m)* is negligible. In Coulomb excitation not only do the velocity of the beam, impact parameter and nuclei involved affect *P(m)*, but the excitation energy also affects *P(m)*, which in turn influences $W(\theta)$. As just seen, the minimum impact parameter and nuclei involved have a

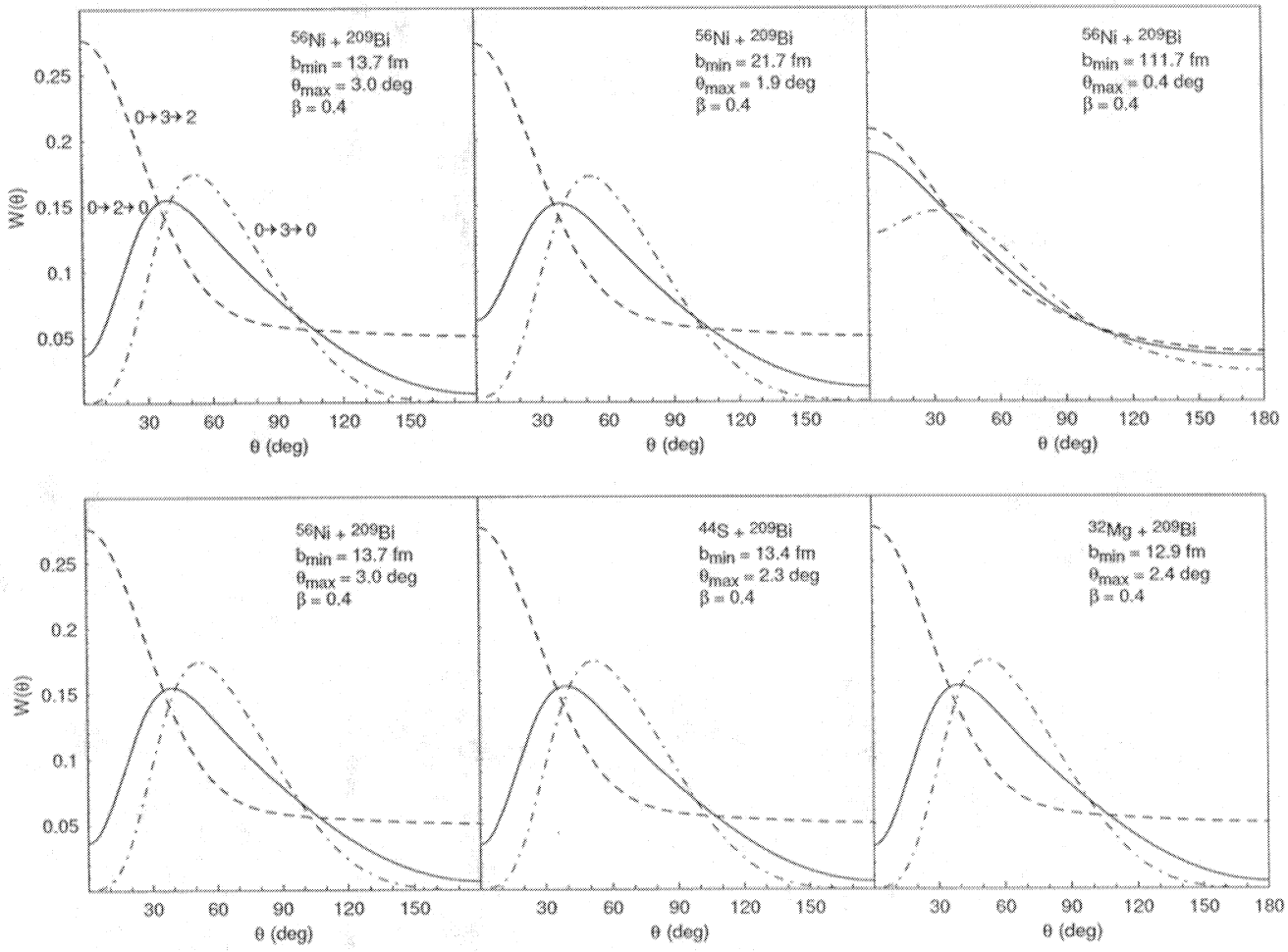

FIG. 11: $W(\theta)$ for Coulomb excitation reactions at 85 MeV/nucleon ($\beta = 0.4$). The top row shows $W(\theta)$ for three different minimum impact parameters, b_{min}. The bottom row shows $W(\theta)$ for three different reactions. The minimum impact parameter is touching spheres plus 2 fm for all three reactions. θ_{max} is the maximum scattering angle of the projectile in the laboratory frame corresponding to b_{min}. As in previous plots, the quadrupole transitions are depicted by solid curves, dipole transitions are dashed curves and octupole transition are dash-dotted curves. The order of the transitions as labeled on the upper left plot is the same for all of the plots in the figure.

minimal effect (within typical impact parameters for Coulomb excitation) on $W(\theta)$, but the excitation energy of the nucleus can have a fairly large effect on $W(\theta)$. In Figure 12, $W(\theta)$ is shown for a quadrupole transition with 1, 2, 5 and 10 MeV excitation energy with the corresponding m substate distributions. $W(\theta)$ is plotted using $\beta = 0.4$ and a minimum impact parameter equal to touching spheres plus 2 fm. Figures 13 and 14 are likewise, except they show dipole and octupole transitions respectively. As the excitation energy increases, the amount of prolate alignment decreases until the alignment becomes oblate. As can be seen in Figure 12, at energies between 5 and 10 MeV there exists an excitation energy where there is 0% alignment. This is significant experimentally because for certain excitation energies where there is no alignment an isotropic angular distribution will be observed, thus yielding no information about excited state spins. Different multipolarity transitions can be

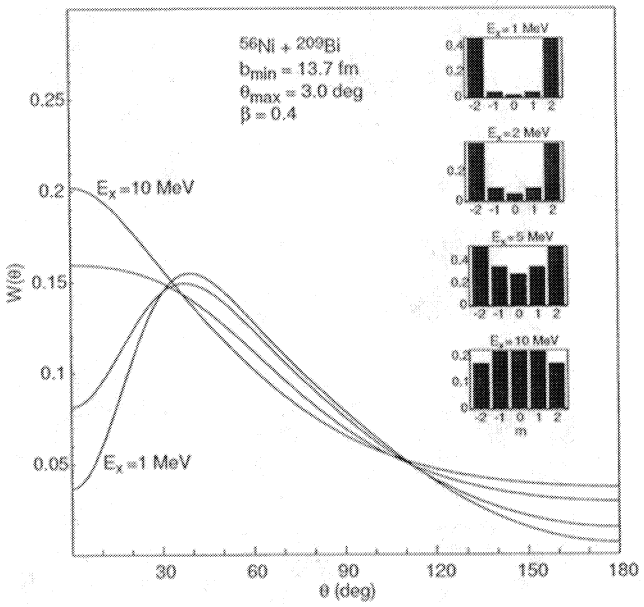

FIG. 12: $W(\theta)$ for quadrupole Coulomb excitation reactions with 1, 2, 5 and 10 MeV excitation energies at 85 MeV/nucleon ($\beta = 0.4$). The minimum impact parameter is equal to touching spheres plus 2 fm. θ_{max} is the maximum scattering angle of the projectile in the laboratory frame corresponding to b_{min}.

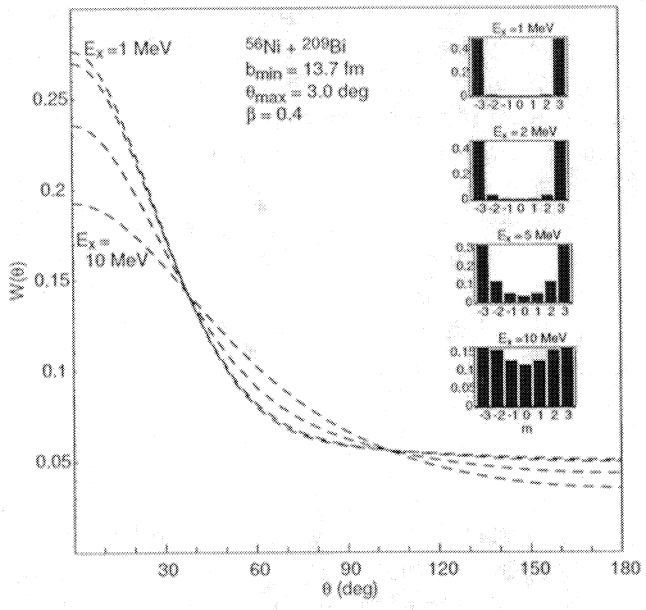

FIG. 13: $W(\theta)$ for dipole Coulomb excitation reactions with 1, 2, 5 and 10 MeV excitation energies at 85 MeV/nucleon ($\beta = 0.4$). The minimum impact parameter is equal to touching spheres plus 2 fm. θ_{max} is the maximum scattering angle of the projectile in the laboratory frame corresponding to b_{min}.

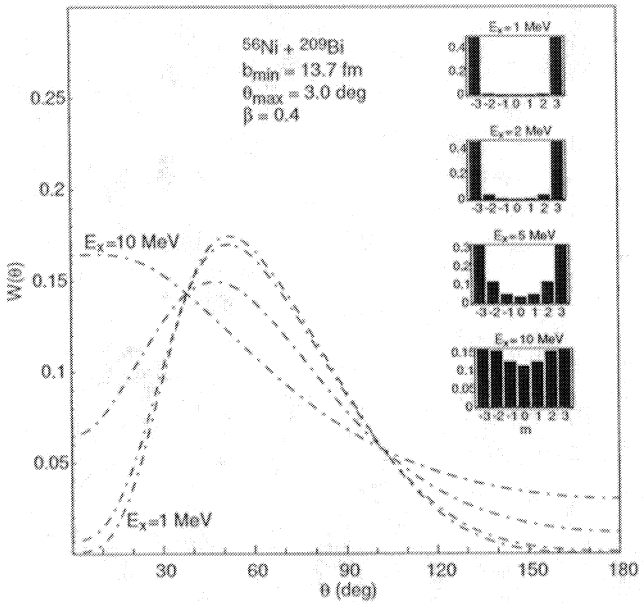

FIG. 14: $W(\theta)$ for octupole Coulomb excitation reactions with 1, 2, 5 and 10 MeV excitation energies at 85 MeV/nucleon ($\beta = 0.4$). The minimum impact parameter is equal to touching spheres plus 2 fm. θ_{max} is the maximum scattering angle of the projectile in the laboratory frame corresponding to b_{min}.

distinguished clearly as long as excitation energies are on the order of a few MeV. Therefore, in intermediate-energy Coulomb excitation, using γ-ray angular distributions to determine multipolarities of γ-ray transitions is feasible.

For intermediate-energy Coulomb excitation performed at $\beta = 0.4$ with an excitation energy of 1 MeV and a minimum impact parameter of touching spheres plus a few femtometers, the relative difference between a quadrupole ($0\rightarrow2\rightarrow0$) and dipole ($0\rightarrow3\rightarrow2$) transition ranges from 88% to 20% if the range of angles around 40° and 100° is avoided. Thus for intermediate-energy Coulomb excitation a minimum of 150 with negligible background in the γ-ray peak at a given angle would be needed to distinguish quadrupole and dipole transitions with a relative difference of 20%. If detectors are placed at very forward (less than 16°) or backward (greater than 142°) angles, the relative difference between a quadrupole and dipole transition is greater than 60%.

V. CONCLUSION

The formalism of γ-ray angular distributions with beams of energies below the Coulomb barrier has been extended to intermediate-energy beams. With proper consideration given to detector placement, it is possible to distinguish stretched quadrupole, dipole and octupole transitions. For intermediate-energy Coulomb excitation, fragmentation and knockout reactions, multipolarities of γ-ray transitions cannot be deduced if detectors are placed at angles around 40° and 100° because at those angles $W(\theta)$ is the same for different multipolarity transitions at $\beta = 0.4$. The relative difference between quadrupole and dipole transitions for specific reaction mechanisms is discussed in section IV. Measuring γ-ray angular distributions of intermediate-energy exotic nuclei is feasible with intermediate-energy Coulomb

excitation, fragmentation and nucleon-knockout reactions and can be used in conjunction with other experimental techniques, such as measuring the momentum distribution of the projectile fragment.

Acknowledgments

We thank P. Gregers Hansen for discussions in regards to nucleon-knockout reactions. This work was supported by the National Science Foundation under grants PHY-9875122, PHY-0070911, and PHY-0110253.

---

[1] W. D. Hamilton, ed., *The Electromagnetic Interaction in Nuclear Spectroscopy* (North-Holland Publishing Company, Amsterdam, 1975).
[2] K. S. Krane, in *Low-Temperature Nuclear Orientation*, edited by N. J. Stone and H. Postma (Elsevier Science Publishers, B.V., 1986), chap. 2.
[3] K. Alder and A. Winther, *Electromagnetic Excitation Theory of Coulomb Excitation with Heavy Ions* (North-Holland Publishing Company, Amsterdam, 1975).
[4] S. Wolfram, *The Mathematica Book* (Wolfram Media/Cambridge University Press, 1996).
[5] A. E. Stuchbery, Nucl. Phys. A **723**, 69 (2003).
[6] T. J. M. Symons, Y. P. Viyogi, G. D. Westfall, P. Doll, D. E. Greiner, H. Faraggi, P. J. Lindstrom, D. K. Scott, H. J. Crawford, and C. McParland, Phys. Rev. Lett. **42**, 40 (1979).
[7] R. Anne et al., Z. Phys. A **352**, 397 (1995).
[8] A. Navin et al., Phys. Rev. Lett. **81**, 5089 (1998).
[9] K. Yoneda et al., Phys. Lett. B **499**, 233 (2001).
[10] T. Motobayashi et al., Phys. Lett. B **346**, 9 (1995).
[11] T. Yamazaki, Nucl. Data A **3**, 1 (1967).
[12] R. M. Diamond, E. Matthias, J. O. Newton, and F. S. Stephens, Phys. Rev. Lett. **16**, 1205 (1966).
[13] E. D. Mateosian and A. W. Sunyar, At. Data and Nucl. Data Tables **13**, 391 (1974).
[14] D. Sohler et al., Phys. Rev. C **66**, 054302 (2002).
[15] G. Neyens et al., Phys. Lett. B **393**, 36 (1997).
[16] W.-D. Schmidt-Ott et al., Z. Phys. A **350**, 215 (1994).
[17] K. Asahi et al., Phys. Rev. C **43**, 456 (1991).
[18] G. A. Souliotis, D. J. Morrissey, N. A. Orr, B. M. Sherrill, and J. A. Winger, Phys. Rev. C **46**, 1383 (1992).
[19] Url: http://www.orau.org/ria/ March 31, 2003.
[20] P. G. Hansen, Phys. Rev. Lett. **77**, 1016 (1996).
[21] P. G. Hansen and J. Tostevin, Annu. Rev. Nucl. Part. Sci. **53** (2003), in press.
[22] P. G. Hansen, *priv. comm.*
[23] H. Simon et al., Phys. Rev. Lett. **83**, 496 (1999).
[24] A. Winther and K. Alder, Nucl. Phys. A **319**, 518 (1979).